Regular Article

ANALYTICAL
AND BIOANALYTICAL
CHEMISTRY
RESEARCH

Published by the
Iranian Chemical Society

***Anal. Bioanal. Chem. Res.**, Vol. 11, No. 3, 343-360, July 2024.*

Fe_2O_3/CuO Hybrid Nanostructures as Electrode Materials for Glucose Detection

Zohreh Shaghaghi*, Alireza Saghebi Shalghuni and Sahar Jafari

Coordination Chemistry Research Laboratory, Department of Chemistry, Faculty of Science, Azarbaijan Shahid Madani University, 5375171379 Tabriz, Iran

(Received 10 February 2024, Accepted 21 April 2024)

In order to solve the disadvantages of using Fe_2O_3 nanoparticles in electrocatalytic processes, in this work, a series of Fe_2O_3/CuO hybrid nanostructures with different molar ratios of Fe^{3+} to Cu^{2+} ions were produced, and their structure was investigated using various methods. Then, the synthesized nanomaterials were used as electrode materials and heterogeneous catalysts for electrochemical detection of glucose in alkaline solution. The results showed that the electrode containing pure Fe_2O_3 shows no significant activity for glucose oxidation. Since Fe(III) oxide contains active electrocatalytic positions, this performance can be due to poor electrical conductivity. Investigations showed that when Fe_2O_3 and CuO nanoparticles are combined, the activity against glucose is improved by reducing the band gap and increasing the electrical conductivity. It was found that the ability of nanocomposites to recognize glucose depends on the molar ratios of Fe^{3+} and Cu^{2+} ions present in the structure, and the highest electrocatalytic performance is observed when the molar ratio of metal ions is equal. Fe_2O_3/CuO (0.5:0.5) nanocomposite shows the best activity for glucose oxidation in terms of high sensitivity, low detection limit, and wide linear range due to its low Tafel slope, low charge transfer resistance, high electrochemically active surface area, low band gap, and high electrical conductivity. In addition, this compound shows high stability, selectivity, and applicability for blood glucose detection with a reasonable recovery rate. In conclusion, the synergistic effects between Fe_2O_3 and CuO increase the number and activity of catalytic sites and rapid charge transfer on the electrode surface and promote the electrocatalytic activity towards glucose.

Keywords: Fe_2O_3 nanoparticles, CuO nanoparticles, Mixed metal oxides, Electrocatalyst, Electrochemistry methods, Non-enzymatic glucose detection

INTRODUCTION

Glucose, as a common carbohydrate, plays a vital role in most of the metabolism of the human body [1]. However, not controlling blood glucose and increasing it causes nerve damage, heart disease, and diabetes. Consequently, glucose measurement is essential for clinical diagnosis and self-care [2,3]. Several innovative techniques including luminescent [4-6], colorimetric [7,8], chromatography [9,10], and electrochemical methods [11,12] have been described for glucose detection. Among them, the electrochemical technique with high sensitivity, portability, and affordable cost is the most attractive method [13]. The electrochemical measurement of glucose can be done in two categories: enzymatic and non-enzymatic [14]. Enzymes such as glucose oxidase, hexokinase, and glucose dehydrogenase are used in enzymatic glucose detection [15]. However, despite their high sensitivity and selectivity, enzymatic glucose biosensors face challenges such as immobility, temperature, pH sensitivity, and limited active sites on material surfaces. Therefore, their catalytic activity decreases with changes in temperature, humidity, pH, and the presence of organic substances [16,17]. On the other hand, non-enzymatic sensors use the direct oxidation of glucose on the surface of the electrodes without the participation of enzymes. Also, non-enzymatic sensors are cost-effective, sensitive, and long-

*Corresponding author. E-mail: shaghaghi@azaruniv.ac.ir

term stable. These advantages make non-enzymatic sensors reliable and attractive for glucose monitoring tools [18]. So far, various nanostructures such as metal oxides [19], LDHs [20], carbon-based nanomaterials [21], MOFs [22,23], and polymers [24] have been reported as non-enzymatic glucose sensors. However, first-row transition metal oxides have received more attention due to their stability, high abundance, and low cost [25]. Among them, magnetic Fe_2O_3 is more favorable as a sensor due to its selective electrocatalytic activity, good thermal conductivity, and biocompatibility [26]. However, Fe_2O_3 has poor hole mobility and its catalytic activity is limited due to poor electrical conductivity [27]. One of the main approaches to increase the catalytic activity of catalysts is to create heterogeneous binary nanostructures. In this way, the products exhibit the intrinsic properties of each metal oxide. Also, some characteristic features such as the number of active sites and the electrochemically active surface area (ECSA) are developed [28]. So far, to improve the electrocatalytic activity of iron oxides against glucose, various nanostructures based on Fe_2O_3 have been investigated. These include porous p-NiO/n-Fe_2O_3 heterostructures [29], $NiFe_2O_4$/NiCoLDH@rGO [30], $ZnFe_2O_4$/α-Fe_2O_3 [26], g-C_3N_4/α-Fe_2O_3 [31], graphene foam/α-Fe_2O_3 [32], Fe_3O_4/rGO [33], Fe_2O_3 ZNRs [34] and so on. However, in these studies, sensors have shown limitations, such as narrow linear range or low sensitivity.

To overcome these drawbacks, CuO is a good candidate to combine with Fe_2O_3. CuO shows high application potential in glucose sensing due to its high p-type conductivity (band gap: ~1.35 eV), excellent catalytic activity, abundance in nature, high electron affinity (4.05 eV), and high ability to increase electrical conductivity [35,36]. In addition, copper oxide can prevent the poisoning of the catalyst surface during the reaction. So far, several researches have been conducted on glucose oxidation with CuO-containing electrocatalysts. For example, studies have shown that binder-free CuO/Cu_2O nanosheets decorated on Cu foil, which have large surface area and high conductivity, can be good candidates for glucose detection with high sensitivity and low detection limit of 1.541 mA mM^{-1} cm^{-2} and 0.57 μM, respectively [37]. In addition to the fact that pure copper oxide can show high activity in glucose detection, it can also improve the electrocatalytic activity of other metal oxides. Incorporation of copper oxide into the structure of other metal oxides improves the catalytic active sites and selectivity. Therefore, the sensitivity for glucose detection increases, and the detection limit decreases [38]. Hierarchical CuO/NiO-C [39], CuO/NiO/ACF nanostructures [35], N-CuO/Cu_2O:NiO [40], CNTs/CuO nanocomposite [41], Au@CuO/V_2CT_xMXene/Laser-induced graphene [42], CuO/Nitrogen-doped Carbon [43] are examples that indicate that CuO has the potential to increase the catalytic performance of electrocatalysts.

In the present study, in order to improve the electrical conductivity of iron oxide and increase its activity against glucose, two-component heterostructures containing copper oxide/iron oxide with different molar ratios of iron to copper ions were prepared by a simple method of co-precipitation and calcination at high temperature. The obtained nanomaterials were utilized in the electrochemical reaction of glucose detection. The results showed that the inclusion of copper oxide in the iron oxide structure reduces the amount of band gap. Therefore, the electrical conductivity increases, and the electron transfer process is accelerated. In addition, the number and activity of the catalytic sites are improved, and as a result, the nanostructures containing CuO and Fe_2O_3 show much higher electrocatalytic activity for glucose detection than pure Fe_2O_3. In fact, the synergistic effects between CuO and Fe_2O_3 in the composite structure make the resulting compound a good conductor for transferring electrons and ions. It was found that when the molar ratio of copper and iron ions is equal, the best electrocatalytic performance is obtained. This study provides ideas for a simple and effective method to significantly improve the electrocatalytic performance of Fe_2O_3 in important processes such as glucose oxidation.

EXPERIMENTAL

Materials and Instruments

All materials in this work are analytical research grade and have been used without any refinements. Iron(III) chloride hexahydrate ($FeCl_3.6H_2O$), copper(II) nitrate trihydrate ($Cu(NO_3)_2.3H_2O$), D-glucose ($C_6H_{12}O_6$), potassium carbonate (K_2CO_3), and sodium hydroxide (NaOH) were obtained from Merck. All other reagents, including fructose (Fr), sucrose (Sc), galactose (Ga), maltose

(Ma), dopamine (DA), ascorbic acid (AA), and citric acid (CA) were purchased from commercial suppliers.

Characterization

Fourier transform infrared (FT-IR) spectroscopy was obtained on a Bruker spectrophotometer in the 400-4000 cm^{-1} using the KBr pellet. The powder X-ray diffraction (PXRD) patterns were conducted on a Tongda model TD-3700 diffractometer (China) with a Cu-K_a source (λ = 1.54056 Å). Field emission scanning electron microscope (FE-SEM) images and EDX/mapping were carried out with a Mira III TESCAN. The X-ray photoelectron spectroscopy (XPS) measurement for the efficient catalyst was recorded by a UHV analysis system equipped with the Al anode (SPECS Co., Germany). Ultraviolet-visible diffuse reflection spectra (UV-Vis DRS) were documented using a JASCO (Japan) model V_670 ultraviolet-visible spectrophotometer fitted with a diffuse reflectance spectroscope.

Synthesis of Nanomaterials

Fe_2O_3/CuO nanocomposites with different molar ratios of Fe^{3+} and Cu^{2+} ions (0.7:0.3, 0.5:0.5, and 0.3:0.7) were synthesized from solutions with constant molarity. First, a 5×10^{-2} M (25 ml) solution of each metal salt was prepared. Then, solutions with different volume ratios were mixed. After that, the pH of the solution was adjusted to 8 using 0.1 M K_2CO_3 solution. The resulting suspension was stirred for 3 h at room temperature. Then, the precipitant was centrifuged, washed three times with distilled water, and transferred into a crucible to be kept in an oven at 80 °C for 12 h. Ultimately, it was left in an electrical furnace at 750 °C for 6 h for further crystallization (see Scheme 1). A similar method was also used to synthesize pure CuO and Fe_2O_3 nanoparticles.

Electrochemical Measurements

Glucose electroanalysis was performed on an Auto-Lab/PGSTAT 101 equipped with Nova 2.1 software and an external rotating disc containing 25 ml of 1 M NaOH electrolyte. For all electrochemical experiments, a three-electrode system containing Ag/AgCl, platinum, and modified carbon paste electrodes (CPEs) was used as reference, auxiliary, and working electrodes, respectively. The electrocatalytic efficiency of synthesized nanomaterials

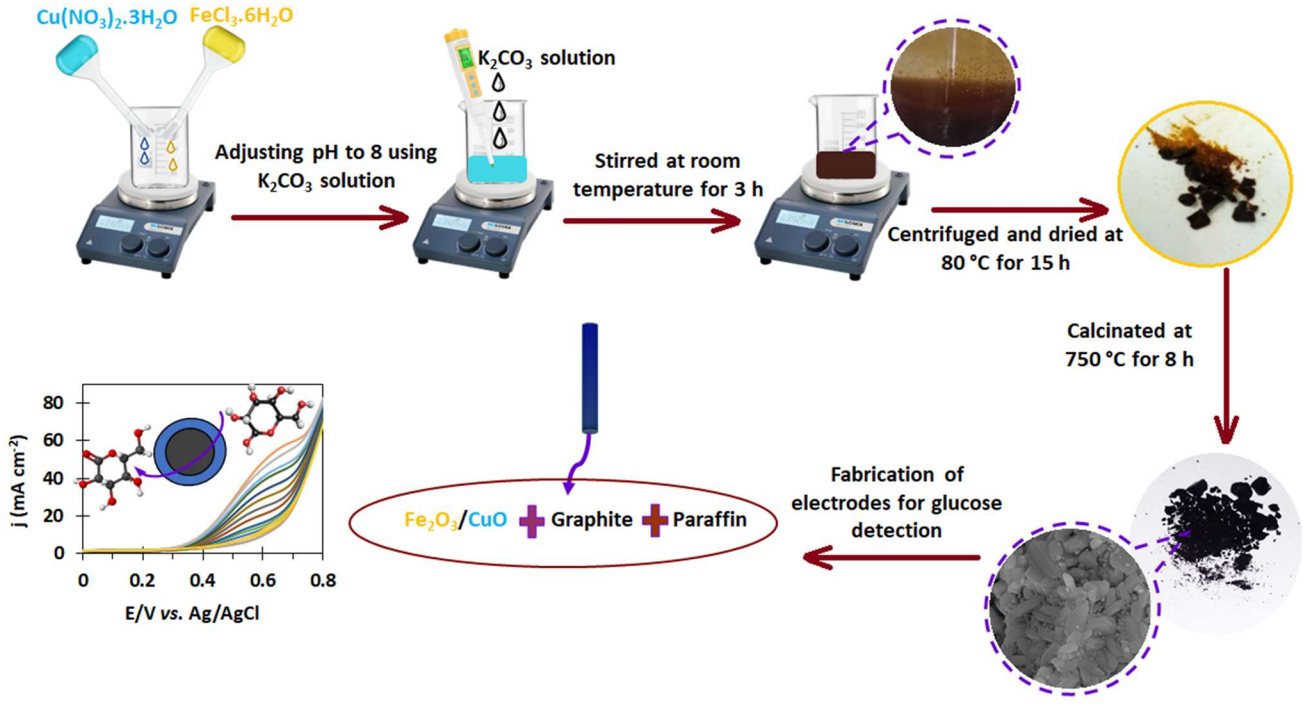

Scheme 1. Synthesis procedure of Fe_2O_3/CuO nanostructures

was investigated by cyclic voltammetry (CV), and amperometry techniques. The optimal potential for glucose detection was calculated from CVs at 75 mV s^{-1} scan rate in the potential range of -0.2 to 0.8 V. To fabricate the working electrodes, a mixture of paraffin (5 mg), each of the nanomaterials (25 mg), and graphite (70 mg) was carefully homogenized. Then, the obtained mixture was filled into a copper wire with a radius of 1.1 mm. The surface of the electrodes was smoothed and washed with distilled water before performing the electrochemical experiments [44,45].

RESULTS AND DISCUSSION

Characterization

Figure 1a depicts FT-IR spectra of Fe_2O_3, CuO, and Fe_2O_3/CuO hybrid nanostructures with different molar ratios of Fe^{3+} and Cu^{2+} ions. For pristine CuO, two characteristic absorption bands at 450 cm^{-1} and 590 cm^{-1} can be attributed to stretching vibrations of Cu-O in the monoclinic structure [46]. Moreover, the spectrum of Fe_2O_3 nanoparticles exhibits firm absorption peaks at 474 cm^{-1} and 554 cm^{-1}, related to the stretching vibrations of the Fe-O bonds of hematite [47,48]. Similarly, the characteristic bands displayed in the range of 424-582 cm^{-1} in the spectrum of hybrid nanostructures are attributed to the stretching vibrations of M-O (M=Cu or Fe) bonds. Also, in the spectrum of all prepared compounds, the broad peak around 3421 cm^{-1} is due to the stretching vibrations of the O-H groups in the water molecules whose bending vibrations can be seen in the range of 1626-1637 cm^{-1} [49].

PXRD pattern was used to confirm the crystalline nature and phase analysis of the synthesized samples. As shown in Fig. 1b, the Fe_2O_3 sample has characteristic peaks at 2θ = 24.32°, 33.32°, 35.68°, 41.04°, 49.60°, 54.16°, 57.80°, 62.48°, and 64.16° are indexed to (012), (104), (110), (113), (024), (116), (018), (214), and (300) planes [50]. These data confirm the presence of the hexagonal phase of hematite α-Fe_2O_3 [51]. The absence of more peaks indicates the high purity of the compound and its single phase [49,52,53]. In the PXRD pattern of CuO, the monoclinic phase is proved with two intense peaks at 2θ = 35.68° (-111) and 38.88° (111). Furthermore, the diffraction peaks at 2θ of 32.64° (110), 48.88° (-202), 53.68° (020), 58.56° (202), 61.72° (-113), 66.64° (-311), and 68.24° (220) is related to the CuO structure. These diffraction peaks match well with JCPDS 80-0076 card [54-57]. As shown in Fig. 1b, the PXRD pattern of Fe_2O_3/CuO nanocomposites shows peaks corresponding to both Fe_2O_3 and CuO peaks, but some changes in the position and intensity of these peaks are seen. When the molar ratio of Fe^{3+} ions to Cu^{2+} ions is 0.7 to 0.3, almost all Fe_2O_3 peaks are seen, but their intensity is reduced compared to pure iron oxide. In contrast, only some low-intensity peaks related to the CuO structure are observed. Since, the molar ratio of Fe ions is high and the prominent peaks of Fe_2O_3 are slightly shifted to high values of 2θ, it can be said that the incorporation of CuO cannot change the structure of iron(III) oxide. For the nanocomposite with an equal molar ratio of metal ions, prominent peaks of both Fe_2O_3 and CuO are observed. This means that in this compound, Fe_2O_3 and CuO act as the main components of the crystal structure. However, the diffraction peaks at 2θ of 35.08° (104) and 36.2° (110) for Fe_2O_3 and 35.72° (-111) and 38.92° (111) for CuO shift to higher 2θ values due to the interaction between Fe, Cu and oxygen ions. Finally, the diffraction pattern of Fe_2O_3/CuO with a molar ratio of 0.3 to 0.7 from Fe^{3+} to Cu^{2+} ions exhibits most CuO characteristic peaks almost with no changes. This means that when Fe_2O_3 is introduced into the CuO lattice, the monoclinic phase of CuO remains unchanged. At the same time, some low-intensity peaks related to Fe_2O_3 are observed, which confirms the presence of Fe_2O_3 in the structure. Eventually, the average crystallite size was calculated using the Debye-Scherr equation and found to be 36.5 nm, 26.8 nm, 26 nm, 31.77 nm, and 36.68 nm for Fe_2O_3, CuO, and Fe_2O_3/CuO with molar ratios of 0.7:0.3, 0.5:0.5, and 0.3:0.7 of Fe to Cu ions, respectively.

UV-Vis DRS technique was employed to investigate the light absorbance properties and the relationship between the electronic band gap and the catalytic activity of the samples. As shown in Fig. 2a, all compounds show a board peak at around 550 nm related to the electron transition of Fe^{2+} to Fe^{3+} and electron excitation from HOMO to LUMO. Also, there are two absorption edges around 360 nm corresponding to the charge transition of O^{2-} to Fe^{3+} [58]. The intensity of these peaks for Fe_2O_3/CuO hybrid nanostructures is higher than that of pure Fe_2O_3. As expected, when several components are combined, the number of defects in the crystal lattice and created holes increase. Therefore, electron transfer and the absorption intensity increase. In addition, the

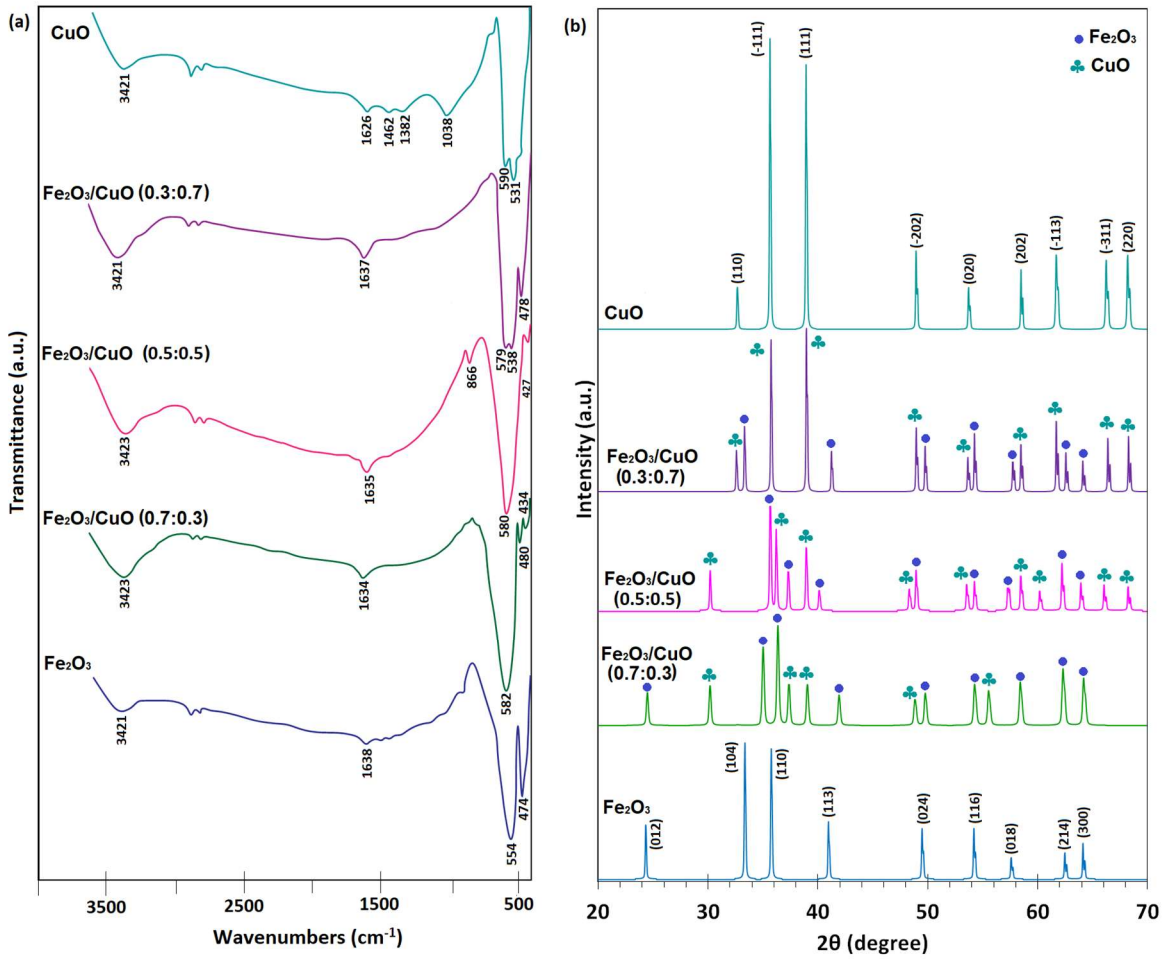

Fig. 1. FT-IR spectra (a) and the PXRD pattern (b) of pure Fe_2O_3, pure CuO, and Fe_2O_3/CuO nanostructures with different molar ratios of Fe^{3+} to Cu^{2+} ions.

broad absorption peak at around 550-800 nm which is clearly observed in the spectrum of CuO/Fe_2O_3 (0.5:0.5) and Fe_2O_3/CuO (0.3:0.7) is assigned to the presence of Cu^{2+} ions [59,60]. The intensity of these peaks gradually increases by adding the molar ratio of Cu^{2+} ions from 0 to 0.7 in the composite structure. The band gap energy (Eg) of the catalysts was determined by the Kubelka-Munk equation and the intersection of the straight line with the x-axis [61]. According to literature, both Fe_2O_3 and CuO have direct electron transition and the value of γ in the Kubelka-Munk equation is equal to 2 [62]. Figure 2b shows the calculated Eg values for Fe_2O_3/CuO heterostructures with different molar ratios. The observed changes in Eg values can be related to the different sizes and crystal defects. Based on the results, Fe_2O_3/CuO with an equal ratio of metal ions exhibit the lowest Eg with 1.85 eV, and Eg for Fe_2O_3/CuO with molar ratios of 0.3 to 0.7 and 0.7 to 0.3 from Fe^{3+} to Cu^{2+} is 2.00 and 2.025 eV, respectively. Meanwhile, pure Fe_2O_3 shows the most considerable band gap value (2.05 eV). The reduction of Eg for Fe_2O_3/CuO nanocomposites compared to pristine iron(III) oxide can be due to the synergistic interactions within the structures and the creation of new energy levels between HOMO and LUMO [61,63].

XPS analysis was used to investigate the oxidation states, surface composition, and electronic interactions in the structure components. The exhaustive scan XPS spectrum confirms the presence of Fe, Cu, and O elements on the surface of Fe_2O_3/CuO (0.5:0.5) (Fig. 3a). According to

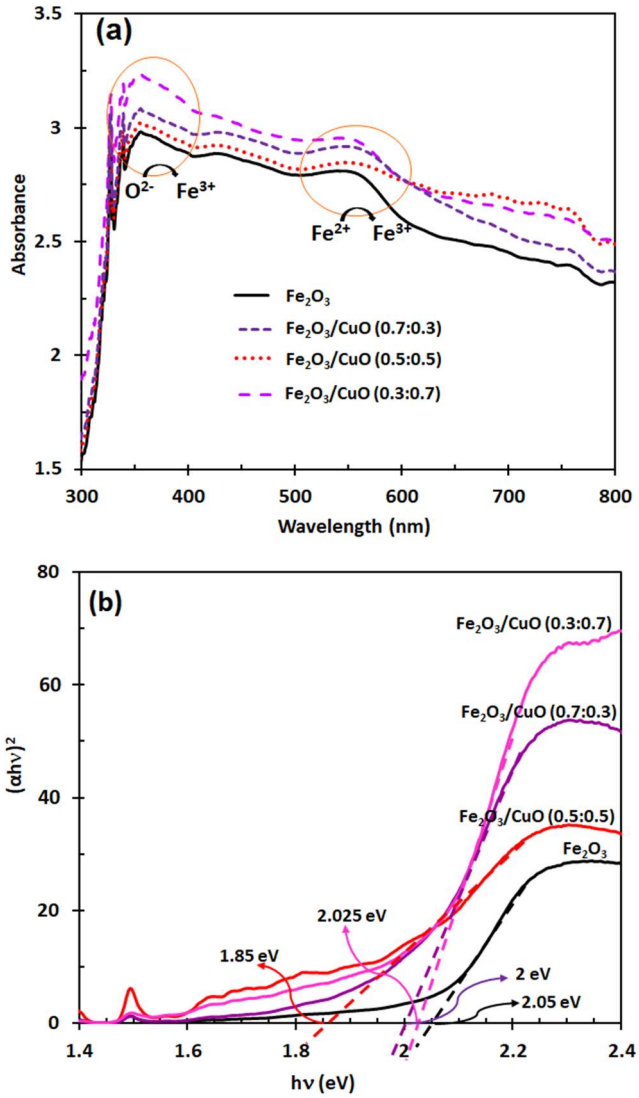

Fig. 2. The UV-Vis-DRS absorbance spectra of the synthesized nanomaterials (a) and calculated band gap for pure Fe_2O_3 and Fe_2O_3/CuO hybrid nanostructures (b).

Fig. 3b, the high-resolution spectrum of Fe has two firm peaks at 711.72 eV and 724.4 eV corresponding to Fe $2p_{1/2}$ and Fe $2p_{3/2}$, respectively. Also, the peak at 717.12 eV is attributed to the Fe $2p_{3/2}$ satellite. The presence of these peaks in the XPS spectrum confirms the +3 oxidation state of Fe in the modified heterostructure [64,65]. The Cu 2p XPS spectrum is shown in Fig. 3c. The prominent peak at 934.3 eV is assigned to Cu^{2+} $2p_{3/2}$ binding energy, with the satellite at 942.5 eV. Moreover, the peak at 954.2 eV and its corresponding satellite at 962.4 eV belong to Cu^{2+} $2p_{1/2}$, which is consistent with previous reports [61,66]. The deconvoluted O 1s spectrum shows two peaks at 530.2 eV and 531.8 eV, corresponding to lattice oxygen, oxygen vacancies, and adsorbed OH^- on the surface (Fig. 3d). This observation indicates the ability of the nanocomposite to absorb hydroxide ions and form active intermediates for glucose detection in an alkaline environment [67]. Finally, the absence of further peaks associated with other elemental oxidation states indicates the purity of the Fe_2O_3/CuO phase.

FE-SEM images and EDX spectra of pure Fe_2O_3 and pristine CuO nanostructures are given in Fig. 4. As considered, both Fe_2O_3 and CuO are composed of nanospheres that are almost uniform in size (Fig. 4a and b). The average size of nanospheres is in the range of 42-52 nm and 38-58 nm for CuO and Fe_2O_3, respectively. The EDX spectrum of CuO nanoparticles displays only copper and oxygen signals, while the spectrum of Fe_2O_3 nanoparticles shows the presence of iron and oxygen elements (Fig. 4c and d). The absence of additional signals in both spectra proves the high crystallinity of the synthesized nanostructures. The morphology, EDX spectrum, and elemental mapping of Fe_2O_3/CuO (0.5:0.5) are shown in Fig. 5. The FE-SEM images demonstrate the aggregated spherical nanoparticles of Fe_2O_3/CuO with diameter between 40 nm to 80 nm (Fig. 5a). The EDX spectrum reveals the characteristic peaks of Fe, Cu, and O and the absence of additional signals specifies the high purity of Fe_2O_3/CuO (Fig. 5b). Finally, the elemental mapping analysis show the distribution of iron, copper and oxygen atoms in the surface of the Fe_2O_3/CuO structure (Fig. 5c).

Electrochemical Glucose Sensing

Cyclic voltammetry experiments. In this part, the electrochemical activity of prepared nanomaterials for glucose electrooxidation was investigated using the CV technique. This method was performed on bare carbon paste and modified carbon paste electrodes by pure Fe_2O_3 and Fe_2O_3/CuO hybrid nanostructures with different molar ratios of Fe^{3+} to Cu^{2+} metal ions. CV experiments were performed in 1 M NaOH electrolyte containing 15 mM

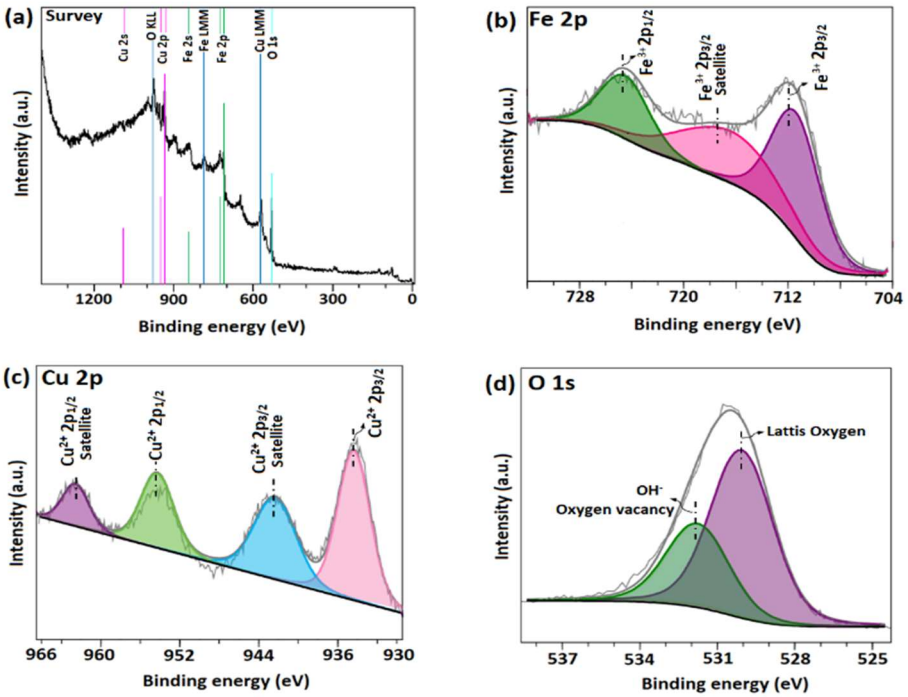

Fig. 3. XPS spectra of Fe_2O_3/CuO (0.5:0.5) (a), high-resolution spectra of Fe 2p (b), Cu 2p (c), and O 1s (d).

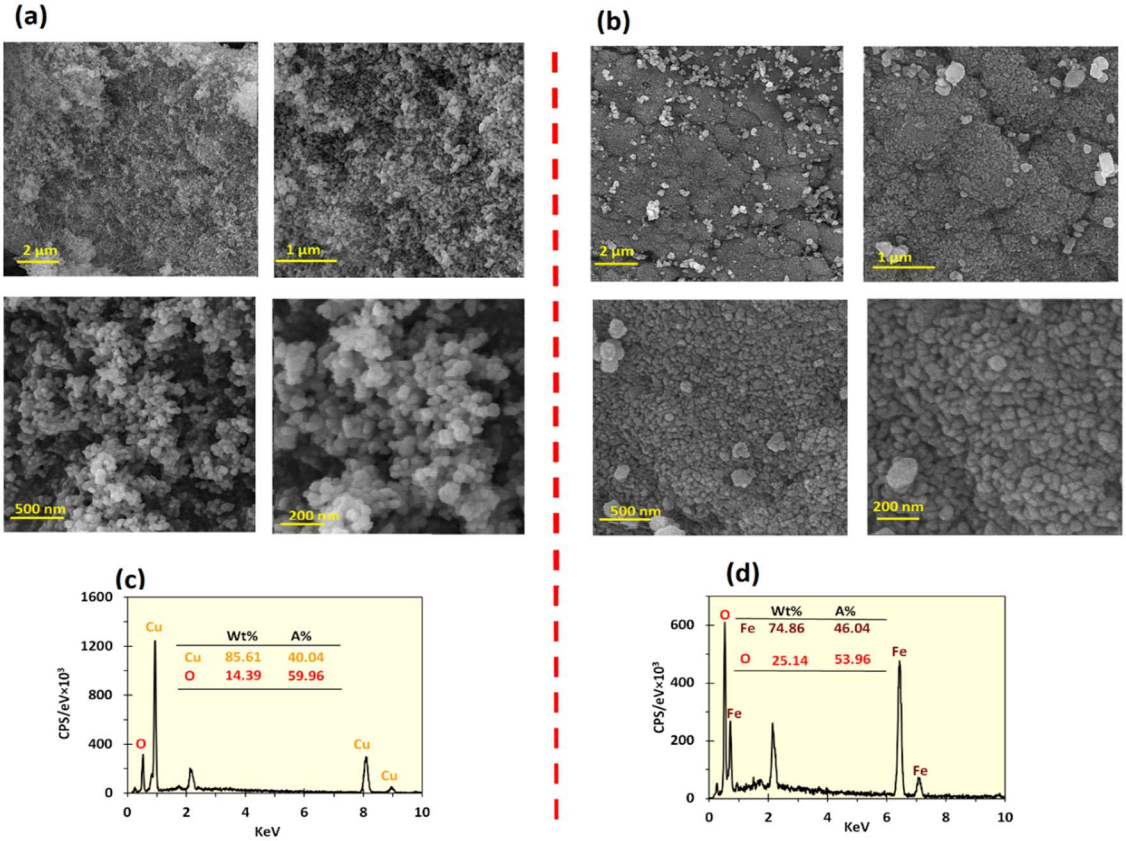

Fig. 4. FE-SEM images (a and b) and EDX spectra (c and d) of CuO and Fe_2O_3 nanostructures, respectively.

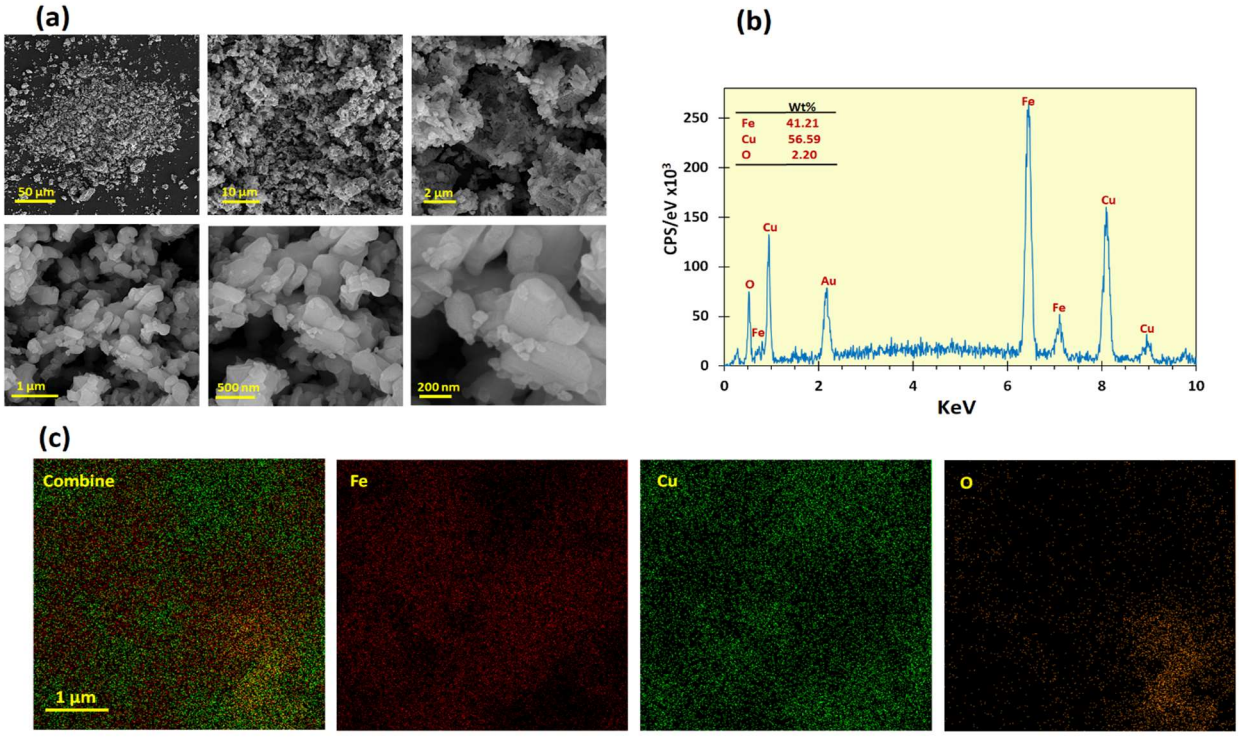

Fig. 5. FE-SEM images (a), EDX spectrum (b), and elemental mapping (c) of Fe_2O_3/CuO (0.5:0.5) hybrid nanostructures.

glucose with a scan rate of 75 mV s^{-1} in the potential range of -0.6 V to 0.8 V *vs.* Ag/AgCl. The CV plots of each electrode with and without glucose are presented in Fig. 6. As can be seen in Fig. 6a, the carbon paste electrode (CPE) in the absence of nanomaterials does not show significant activity for glucose electro-oxidation, and CVs before and after addition of 15 mM glucose are similar. Also, there is no detectable oxidation peak towards glucose on the modified electrode by Fe_2O_3 (Fig. 6b). Although it has been proven that Fe_2O_3–based electrodes have electrocatalytic active sites for oxidation of glucose in alkaline solutions, this behavior can be related to the low electrical conductivity and high Eg value of pure Fe_2O_3. The catalytic performance of modified electrodes by Fe_2O_3/CuO hybrid nanostructures with different molar ratios of metal ions is given in Fig. 6c-e. As considered, when copper oxide is introduced into the Fe_2O_3 structure, the current density in the glucose oxidation potential range increases with the addition of glucose to the electrolyte solution. The peak related to glucose oxidation clearly appears when the molar ratio of Fe^{3+} ions to copper ions is 0.5 to 0.5 and 0.3 to 0.7. All nanocomposites show an addition in current density at the potential of about 0.5 V *vs.* Ag/AgCl, which is assigned to glucose oxidation. As shown, the Fe_2O_3/CuO hybrid nanostructure with an equal molar ratio of metal ions displays the highest current density in the range of glucose oxidation potential (about 0.5 V) among other nanocomposites. The improved electrocatalytic activity of Fe_2O_3/CuO hybrid nanostructures compared to pure Fe_2O_3 can be related to the synergistic effects between the two metal oxide components participating in the composite structure. These effects increase electrical conductivity, fast charge transfer, and catalytic sites and their activity and sensitivity for glucose detection [68].

According to the literature [69-72], in the process of glucose detection on the CuO electrode surface, the production of Cu^{III} is impossible due to kinetic and thermodynamic limitations. However, a suitable anodic potential creates a few vacancies (h^+) on the electrode surface. These vacancies subsequently interact with the hydroxyl groups (OH^-) on the surface, resulting in the formation of hydroxyl radicals ($OH^{\bullet}_{ads}$). Hydroxyl radicals in turn react with other hydroxyl groups. Then glucose reacts

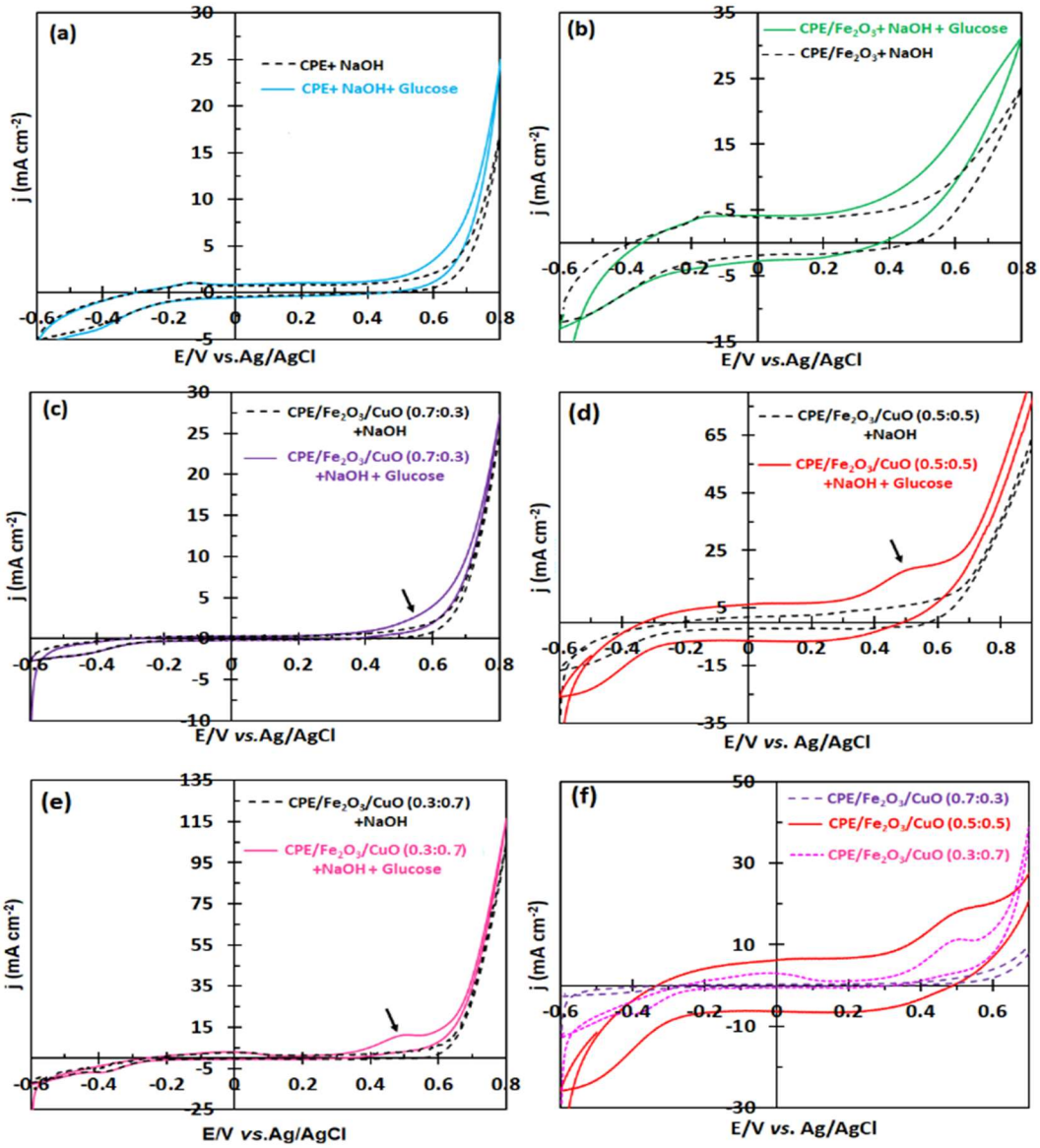

Fig. 6. CVs of bare (a), pure Fe_2O_3 (b), and Fe_2O_3/CuO electrodes (c-e) in the absence and presence of 15 mM glucose and comparison of CVs for all electrodes in the presence of 15 mM glucose (f); scan rate = 75 mV s^{-1}, electrolyte = NaOH (25 ml, 1 M).

with this surface with the help of active hydrogen and the oxidation process is carried out. On the other hand, Fe_2O_3 nanoparticles can oxidize glucose in alkaline electrolytes, leading to gluconolactone and FeO. Subsequently, FeO interacts with OH^- ions to form Fe_2O_3 [73-75]. In the Fe_2O_3/CuO nanocomposite structure, both Fe_2O_3 and CuO are present in catalytic sites and the interaction between them increases the active catalytic sites and improves electrocatalytic activity for glucose oxidation. Also, based on the DRS results, when CuO is introduced into the Fe_2O_3 structure, the band gap value decreases. Fe_2O_3/CuO (0.5:0.5) has the lowest band gap among all tested nanocomposites. This leads to improved electrical conductivity of this compound, faster electron transfer, and unique activity in the glucose electro-oxidation process.

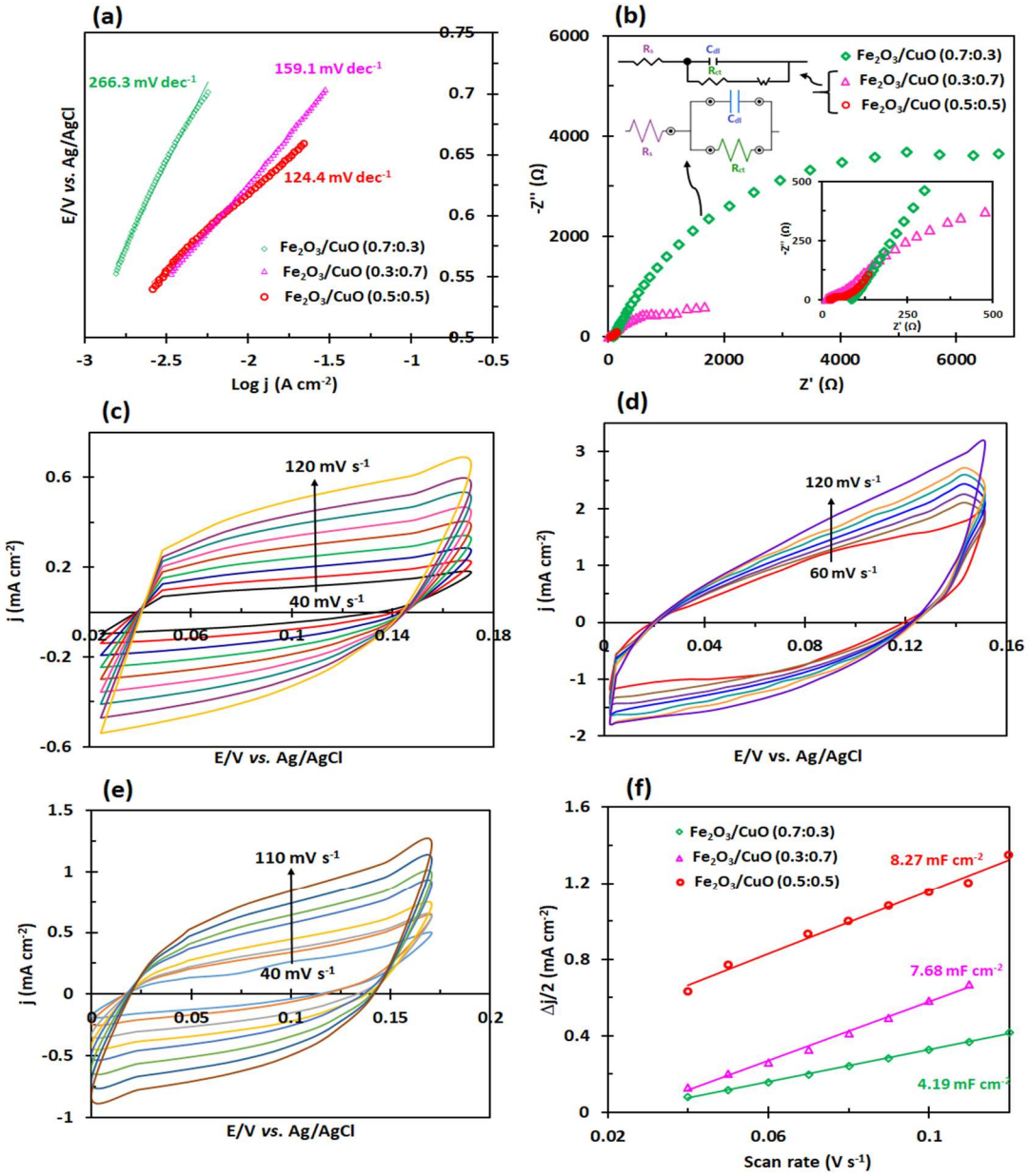

Fig. 7. Tafel plots of Fe_2O_3/CuO hybrid nanostructures, obtained CVs in the presence of 15 mM glucose at the low scan speed of 5 mV s^{-1} (a), Nyquist plots obtained at a constant potential of 0.48 V and their corresponding equivalent circuits (b), CV curves of Fe_2O_3/CuO hybrid nanostructures (c, d, and e) in the non-faradic region of 0-0.15 V at different scan rates of 40-120 mV s^{-1}, and computed C_{dl} for electrodes (f).

One of the critical factors in investigating the electrocatalytic activity of electrodes against glucose oxidation is determining the Tafel slope. The kinetics of the electrochemical process can be evaluated based on the slope of the Tafel plot, and a slight slope reveals a fast electron transfer rate. As shown in Fig. 7a, the lowest Tafel slope value is achieved for the Fe_2O_3/CuO (0.5:0.5) electrode (124 mV dec^{-1}), indicating its desirable kinetic performance compared to other electrodes. For further investigation, Nyquist plots are plotted at the operating frequencies of

10^{-1} to 10^5 Hz (Fig. 7b). Also, their corresponding equivalent circuits is given in Fig. 7b (inset) [76,77]. The results display that the Fe_2O_3/CuO (0.5:0.5) electrode has the smallest semicircular diameter and the lowest charge transfer resistance for the oxidation of glucose among all tested hybrid nanostructures. The R_{ct} for this electrode has the lowest value (2.32 Ω cm^2), while the value for Fe_2O_3/CuO (0.7:0.3) and Fe_2O_3/CuO (0.3:0.7) electrodes is 404.47 and 59.84 Ω cm^2, respectively. In addition, the R_s values for Fe_2O_3/CuO (0.5:0.5) is 0.741 Ω cm^2, while this value for Fe_2O_3/CuO (0.7:0.3) and Fe_2O_3/CuO (0.3:0.7) is 3.53 and 1.94 Ω cm^2, respectively. Finally, the electrochemically active surface area (ECSA) was used for further insight into the origin of the catalytic activity as well as synergistic effects. Generally, ECSA is calculated from the formula ECSA = C_{dl}/C_s, where C_s and C_{dl} are specific capacitance and double-layer capacitance, respectively. Since the value of C_s cannot be easily calculated, ECSA cannot be calculated precisely. Nevertheless, because C_{dl} has a proportional relationship with ECSA, it can be considered that as C_{dl} increases, the value of ECSA also increases. As shown in Fig. 7c-f, C_{dl} is calculated in the non-faradic region of CVs with different scan rates. As shown in Fig. 7f, the calculated C_{dl} for Fe_2O_3/CuO (0.5:0.5) is 8.23 mF cm^{-2}, which is higher than the C_{dl} of other prepared nanocomposites (4.19 mF cm^{-2} for Fe_2O_3/CuO (0.7:0.3) and 7.68 mF cm^{-2} for Fe_2O_3/CuO (0.3:0.7)). This indicates that Fe_2O_3/CuO (0.5:0.5) has higher active catalytic sites for glucose oxidation than other hybrid nanostructures. Although the electrochemical experiment results show that Fe_2O_3/CuO nanocomposites generally act better than pure Fe_2O_3 in glucose oxidation, the synergistic interactions have the greatest effect when the molar ratio of Fe^{3+} ions to Cu^{2+} ions in the composite structure is equal. Consequently, this sensor shows the lowest Tafel slope, the lowest charger transfer resistance, and the highest ESCA compared to other studied sensors and as will be discussed further, it shows the highest sensitivity and the lowest detection limit for glucose detection [78].

Figure 8 shows the CV plots of the electrode modified with Fe_2O_3/CuO (0.5:0.5) at a scan speed of 75 mV s^{-1} and in the potential range of -0.6 V to 0.8 V *vs*. Ag/AgCl in the presence of 1 M NaOH and 0-40 mM glucose. In the absence of glucose, the oxidation peak is not visible. However, when

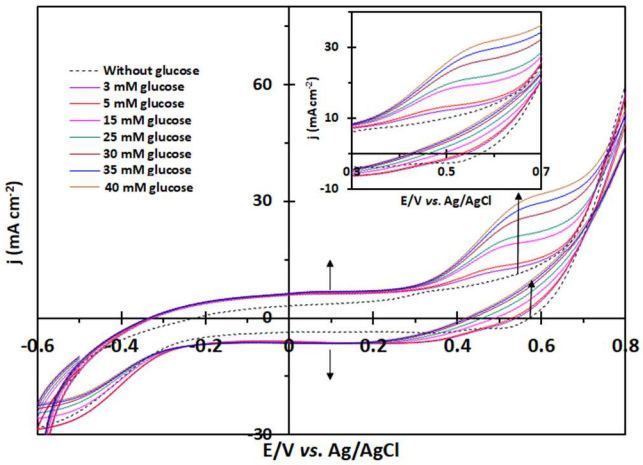

Fig. 8. CVs of Fe_2O_3/CuO (0.5:0.5) in the presence of different concentrations of glucose.

glucose is added to the solution, an oxidation peak occurs at about 0.45 V *vs*. Ag/AgCl. The current density of this anodic peak gradually increases with increasing glucose concentration and slowly shifts towards positive potentials. Considering the results of CV techniques, the optimal potential of 0.55 V was selected for Fe_2O_3/CuO (0.5:0.5) to investigate the sensitivity and limit of detection (LOD) for glucose in the presence of this electrocatalyst.

Amperometry experiments. To determine the linear range, LOD, and sensitivity of electrocatalysts for glucose detection, amperometry experiments were conducted using carbon paste electrodes modified with Fe_2O_3/CuO nanocomposites at the optimum potential. According to the CV diagrams, the optimum potential for Fe_2O_3/CuO with molar ratios of 0.7 to 0.3, 0.5 to 0.5, and 0.3 to 0.7 from Fe^{3+} to Cu^{2+} ions was determined to be 0.6, 0.55, and 0.5 V *vs*. Ag/AgCl. Figure 9a, c, and e show the current-time plots of Fe_2O_3/CuO hybrid nanostructures with different molar ratios of metal ions. As considered, The Fe_2O_3/CuO (0.5:0.5) displays higher amperometry currents in the presence of different glucose concentrations than other nanocomposites. In all cases, the amperometry response increased rapidly with the addition of different glucose concentrations and reached a steady state within approximately 4 s. As shown in Fig. 9b, d, and f, the current density increases linearly with the addition of different glucose concentrations. For all the

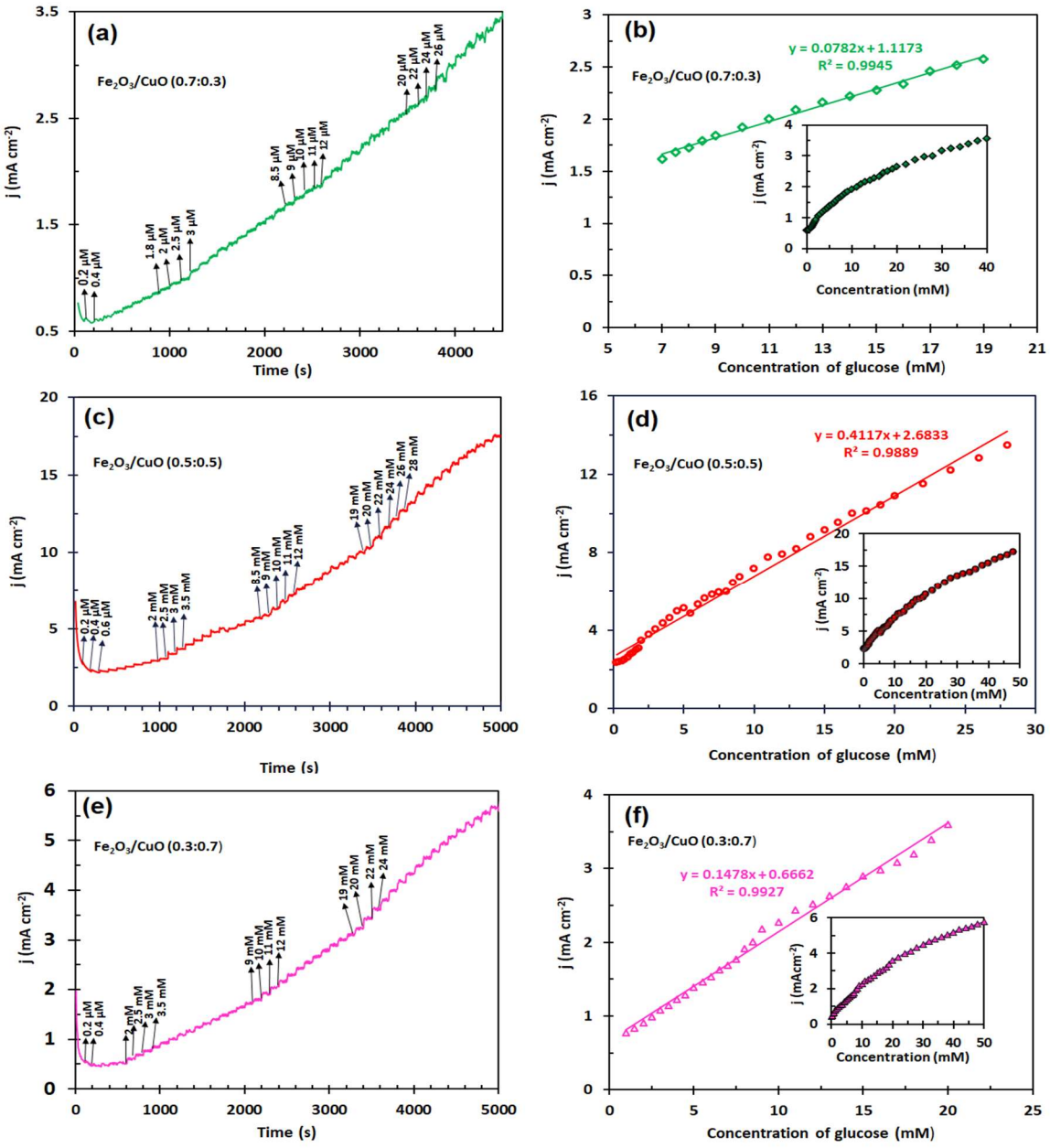

Fig. 9. Amperometric response of Fe_2O_3/CuO hybrid nanostructures with different molar ratios of Fe^{3+} and Cu^{2+} ions towards different concentrations of glucose (0-50 mM) in 1 M NaOH electrolyte solution (25 ml) at optimal potentials between 0.5-0.6 V (a, c, and e) and the plots of current density against different concentrations of glucose and corresponding calibration curves (b, d, and f).

modified electrodes, the deviation from the linear mode occurs at higher concentrations of glucose. This could be related to the saturation of active catalytic sites on the electrode surface [71]. Interestingly, the nanocomposite with an equal molar ratio of metal ions shows a wide linear range compared to other electrocatalysts. For Fe_2O_3/CuO (0.5:0.5), the deviation from the linear range is observed at glucose concentrations higher than 28 mM, while for Fe_2O_3/CuO

(0.7:0.3) and Fe_2O_3/CuO (0.3:0.7), this deviation occurs at higher concentration of 20 mM. These results are in good agreement with the calculated C_{dl} values. Fe_2O_3/CuO (0.5:0.5) has the highest electrochemically active surface area and active catalytic sites among all tested electrodes, and therefore, a saturation of active sites occurs at higher amounts of glucose. In the next step, the linear range and sensitivity of electrocatalysts for glucose were determined using calibration curves. As can be seen from Fig. 9b, the Fe_2O_3/CuO (0.5:0.5) electrode shows a wide linear range between 0.2 and 28 mM of glucose, which is associated with a sensitivity of 411.7 μA mM^{-1} cm^{-2} and a low detection limit of 0.2 μM. Furthermore, the apparent Michaelis-Menten constant (Km), which indicates the glucose-substrate kinetics for the sensor, can be calculated from the electrochemical version of the Lineweaver-Burk equation [79,80].

$$1/iss = 1/imax + 1/K_m\ C$$

In this equation, i_{ss} is the steady state current after glucose addition, C is the bulk concentration of glucose and i_{max} is the maximum current measured under saturated substrate conditions. The K_m value of the glucose sensor (Fe_2O_3/CuO (0.5:0.5)) was determined by the steady-state amperometric response curve to be 5.49 mM, which was smaller than the K_m values calculated for Fe_2O_3/CuO (0.7: 0.3) (9.33 mM) and Fe_2O_3/CuO (0.3: 0.7) (8.14 mM). As shown in Table 1, the Fe_2O_3/CuO (0.5:0.5) electrode displays the widest liner range, the highest sensitivity, and the lowest glucose detection limit compared to other modified electrodes. In addition, this compound shows good performance in the oxidation of glucose compared to some previous works. Therefore, subsequent tests such as stability, selectivity, and

Table 1. Comparison of Non-enzymatic Glucose Sensors and Biosensors Based on Fe_2O_3

Compounds	Sensitivity (μA mM^{-1} cm^{-2})	Linear range (mM)	LOD (μM)	Ref.
Fe_2O_3/CuO (07:0.3)	78.20	7-19	51	This work
Fe_2O_3/CuO (05:0.5)	411.7	0.2-28	0.2	
Fe_2O_3/CuO (03:0.7)	147.8	1-20	11	
$ZnFe_2O_4$/Fe_2O_3@Gr	609	1-10	-	[26]
NiO/Fe_2O_3	1437 μA mM^{-1}	-	1.03	[29]
$Ni_2Fe_2O_4$/NiCoLDH@rGO	111.86	3.5×10^{-5}-4.5×10^{-3}	1.29×10^{-5}	[30]
gC_3N_4/α-Fe_2O_3	105.75	0.002-2.4	0.4	[31]
ITO/HNC/CS/GOx	20.03	1-5 mM	71.6	[32]
Fe_2O_3 ZNRs	105.75	0.05-18	12	[34]
α-Fe_2O_3/Nickel foam	10356	0.005-0.2	0.87	[73]
α-Fe_2O_3 nanostructures	85.384	0.003-33	1	[81]
α-Fe_2O_3 nanoparticles	30.89	1-10	-	[82]
ZnO NRs/Fe_2O_3/nafion	0.052 μA cm^{-2}	-	0.95 mM	[83]
Fe_2O_3-NPs/P4VP-co-PAN	1382.5	0.0025-0.58	0.58	[84]
Polypyrrole/$ZnFe_2O_4$	145.36	0.01-8	-	[85]
Fe_3O_4−CS−CD	23.59	40 μM-1.04 mM	19.30	[86]
Nafion/α-Fe_2O_3/rGO/GCE	327.92	1-5 mM	0.6 mM	[87]
rGO/Fe_3O_4/GO_x/GCE	2.645 μA mM^{-1}	0.5-10	106.5	[88]
Nafion/GOx/γ-Fe_2O_3 NP–0.25 CA	5.81 995.57	5.0 μM-20.0 mM 1.1-5 μM	- 0.05	[89]

Abbreviations: HNC = hetero-nanocomposite of 1D α-Fe_2O_3 nanowires; Gr: graphite; ZNRs: ZnO nanorods; P4VP-co-PAN: poly(4-vinylpyridine)-co-poly(acrylonitrile); CS: Chitosan; CA: citric acid.

real sample analysis were performed in the presence of this electrocatalyst.

As is apparent, there are many electroactive species in the real sample which may reduce the accuracy of glucose detection. Therefore, selectivity is one of the critical tests during electrochemical glucose oxidation to develop an electrochemical enzyme-free glucose sensor. The glucose concentration in the blood is usually in the range of 3 to 8 mM, which is significantly higher than the concentration of possible interferences. In order to check the selectivity, the experiments were performed in 1 M NaOH solution with an applied potential of 0.55 V in the presence of 5 mM glucose and 0.2 mM of interferences, such as Fr, Sc, Ga, Ma, DA, AA, CA, NaCl, urea, and ethanol. According to Fig. 10a, a noticeable signal is observed when glucose is added. However, no significant response is observed for interference agents, which leads to the high selectivity of Fe_2O_3/CuO (0.5:0.5) in glucose detection.

The amperometry method was also utilized to check the durability and long-term stability of the Fe_2O_3/CuO (0.5:0.5) electrode. Figure 10b shows the long-term stability as assessed by dividing the amperometry response (I) against 5 mM glucose in 1 M NaOH by the amperometry current in the absence of glucose (I_0) for 19 days, indicating the current signal does not show a significant decrease during this time. Therefore, this electrode has high stability. Also, the durability and stability of the Fe_2O_3/CuO (0.5:0.5) was studied by amperometry technique for 1000 s in the presence of 5 mM glucose in 25 ml 1 M NaOH (Fig. 10c). As shown, the amperometry current increases rapidly after the addition of glucose, remains constant for 1000 s, and then increases again with the addition of glucose, indicating its high durability. Moreover, the robustness of the electrode was confirmed through interday (during five days) and intraday (five times) measurements by recording the current response of Fe_2O_3/CuO (0.5:0.5) hybrid nanostructures in the presence of 5 mM glucose. The interday and intraday tests yielded t-values of 1.976 and 1.542, respectively. These findings suggest that there were no systematic errors detected by the t-test calculation, with P = 0.05 ($|t|_{critical,4}$ = 2.78) [90].

Detection of real samples can demonstrate the application of designed electrochemical sensors. In this case, the standard addition method was used to test the reliability of Fe_2O_3/CuO (0.5:0.5) in human blood serum [91,92]. Blood serum was obtained from a nearby hospital and deproteinized using methanol at a volume ratio of 1:3 serum to methanol before analysis. The amperometry test at E_{appl} = 0.55 V was carried out by adding 250 µl of serum to 25 ml of 1 M NaOH and injecting different concentrations of pure glucose into the solution at intervals of 100 s. Finally, the glucose concentration in blood serum was determined by plotting the current response against different glucose concentrations. This experiment was repeated three times. It was revealed that the concentration of glucose in blood serum is 4.23 mM.

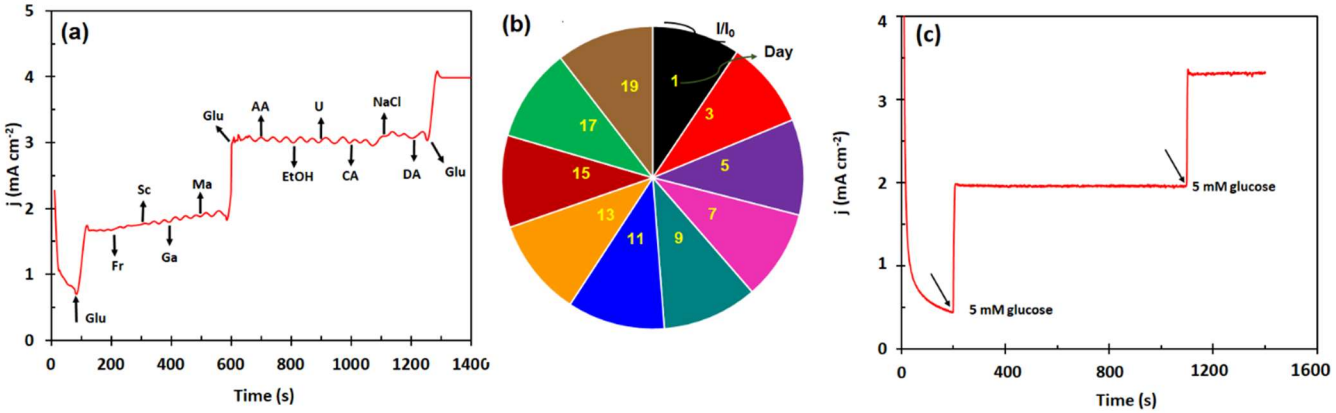

Fig. 10. The selectivity test for glucose detection by the Fe_2O_3/CuO (0.5:0.5) nanocomposite after adding 5 mM glucose and 0.2 mM of carbohydrate and non-carbohydrate interferences (a), the durability test for Fe_2O_3/CuO (0.5:0.5) in the presence 5 mM glucose for 1000 s (b), and the stability test for Fe_2O_3/CuO 0.5:0.5 containing 5 mM glucose by amperometry technique for 19 days (c) (All experiments were performed in 25 ml of 1 M NaOH).

Table 2. Determination of Glucose in Human Blood Serum Sample for Fe_2O_3/CuO (0.5:0.5) (Glucose Concentration in Blood Sample = 4.23 mM)

Sample	Spiked glucose (mM)	Found glucose (mM)	RSD% (n = 3)	Recovery%	Student's t-test
1	0.5	4.72	1.12	99.87	0.32
2	1	5.17	1.13	98.85	1.67
3	1.5	5.75	0.69	100.34	0.87

To test the accuracy and recovery of the method, three different serum samples (3 ml) were spiked with pure glucose solutions (0.5, 1, and 1.5 mM). Then, the amperometry test was done by adding 300 µl of serum to 25 ml of 1 M NaOH and injecting different concentrations of pure glucose into the solution at intervals of 100 s. Finally, the calibration curves were plotted to determine the glucose concentration. As shown in Table 2, the recovery rate changed from 98.85 to 100.34%, and the RSD value from three independent repetitions was calculated below 2%, which indicates the excellent repeatability of this nanomaterial. Also, the calculated student's t-test values in different concentrations suggest that there is no substantial systematic error in analyzing the real sample. This conclusion is based on comparing the calculated |t| value with the P = 0.05 ($|t|_{critical,2}$ = 4.30) in three repeated measurements [90]. These results indicate that the fabricated electrode can be a promising candidate for detecting glucose in human serum.

CONCLUSION

In the present study, to increase the electrocatalytic activity of Fe_2O_3 nanoparticles in the glucose detection process, Fe_2O_3/CuO hybrid nanostructures with different molar ratios of Fe^{3+} to Cu^{2+} ions were successfully synthesized using a simple co-precipitation technique. The results showed that in the hybrid nanostructures of CuO and Fe_2O_3, the synergistic effects between the two metal oxides improve the electrical conductivity, and fast charge transfer and increase the active catalytic positions, thus increasing their activity for glucose. Among all tested Fe_2O_3/CuO nanocomposites, the structure with the equal molar ratio of Fe^{3+} to Cu^{2+} ions showed the lowest Tafel slope and charge transfer resistance due to its low band gap value, which indicated that this compound has a desirable kinetic for glucose oxidation. In addition, this compound has the largest C_{dl} value, indicating its more catalytic active sites for reaction. Further experiments revealed that the Fe_2O_3/CuO (0.5:0.5) shows the highest current amperometry response for glucose and has the highest sensitivity, good stability, a wide linear range, a low detection limit, and excellent selectivity for glucose detection. Also, the practical detection capability of Fe_2O_3/CuO (0.5:0.5) was confirmed *via* real sample analysis with a reasonable recovery percentage. Finally, the cost-effective and simple method of producing these heterostructures makes them promising candidates for glucose monitoring applications.

ACKNOWLEDGMENT

The authors thank Shahid Madani University of Azerbaijan for supporting this work.

REFERENCES

[1] R. Wang, X. Liu, Y. Zhao, J. Qin, H. Xu, L. Dong, S. Gao, L. Zhong, Microchem. J. 174 (2022) 107061.

[2] S.M. Babulal, S.-M. Chen, R. Palani, K. Venkatesh, A.S. Haidyrah, S.K. Ramaraj, C.-C. Yang, C. Karuppiah, Colloids Surf. A: Physicochem. Eng. Asp. 621 (2021) 126600.

[3] O. Adeniyi, N. Nwahara, D. Mwanza, T. Nyokong, P. Mashazi, Sens. Actuators B Chem. 348 (2021) 130723.

[4] R. Zhang, L. Liu, W. Li, X. Luo, F. Wu, Colloids Surf. B Biointerfaces 222 (2023) 113125.

[5] Y. Sun, T. Shu, J. Ma, Q. Dai, P. Peng, Z. Zhou, X. Zhou, L. Su, X. Zhang, Anal. Chem. 94 (2022) 3408.

[6] F. Momeni, S.M. Khoshfetrat, H. Bagheri, K. Zarei,

Biosens. Bioelectron. 250 (2024) 116078.
[7] B.S. Bharat, A.D. Bagde, A.R. Babu, Mater. Sci. Eng. B 298 (2023) 116886.
[8] R. Baretta, V. Gabrielli, M. Frasconi, ACS Appl. Nano Mater. 5 (2022) 13845.
[9] S. Yeganeh-Zare, K. Farhadi, S. Amiri, Food Chem. 370 (2022) 131015.
[10] M. Soyseven, B. Sezgin, G. Arli, J. Food Compos. Anal. 107 (2022) 104400.
[11] T.-T. Wang, X.-F. Huang, H. Huang, P. Luo, L.-S. Qing, Adv. Sens. Energy Mater. 1 (2022) 100016.
[12] H. Teymourian, A. Barfidokht, J. Wang, Chem. Soc. Rev. 49 (2020) 7671.
[13] Y. Zhang, Y.-Q. Liu, Y. Bai, X. Li, W. Chu, Appl. Surf. Sci. 539 (2021) 148235.
[14] Y.X. Niu, X. Li, J. Pan, Y. He, F. Qiu, Y. Yan, RSC Adv. 6 (2016) 84893.
[15] K.E. Toghill, R.G. Compton, Int. J. Electrochem. Sci. 5 (2010) 1246.
[16] P. Si, Y. Huang, T. Wang, J. Ma, RSC Adv. 3 (2013) 3487.
[17] M.H. Hassan, C. Vyas, B. Grieve, P. Bartolo, Sensors, 21 (2021) 4672.
[18] S. Liu, X. Jiang, G.I. Waterhouse, Z.-M. Zhang, L.-M. Yu, J. Electroanal. Chem. 897 (2021) 115558.
[19] Q. Dong, H. Ryu, Y. Lei, Electrochim. Acta 370 (2021) 137744.
[20] H. Sohrabi, E. Dezhakam, E. Nozohouri, M.R. Majidi, Y. Orooji, Y. Yoon, A. Khataee, Chemosphere, 309 (2022) 136633.
[21] G. Balkourani, T. Damartzis, A. Brouzgou, P. Tsiakaras, Sensors, 22 (2022) 355.
[22] H. Sohrabi, F. Maleki, P. Khaaki, M. Kadhom, N. Kudaibergenov, A. Khataee, A review of status and prospects, Biosensors, 13 (2023) 347.
[23] Y. Zhang, Q. Lin, Y. Song, J. Huang, M. Chen, R. Ouyang, S.-Y. Liu, Z. Dai, Chemosensors 11 (2023) 429.
[24] M. Yadav, G. Singh, S. Lata, J. Anal. Test. 6 (2022) 274.
[25] G.A. Naikoo, H. Salim, I.U. Hassan, T. Awan, F. Arshad, M.Z. Pedram, W. Ahmed, A. Qurashi, Front. Chem. 9 (2021) 748957.
[26] D. Neravathu, A.R. Paloly, P. Sajan, M. Satheesh, M.J. Bushiri, Diam. Relat. Mater. 106 (2020) 107852.
[27] F. Liu, P. Wang, Q. Zhang, Z. Wang, Y. Liu, Z. Zheng, X. Qin, X. Zhang, Y. Dai, B. Huang, Electroanalysis, 31 (2019) 1809.
[28] Y. Yang, C. Zhu, Y. Zhang, Y. Xie, L. Lv, W. Chen, Y. He, Z. Hu, J. Phys. Chem. Solids 148 (2021) 109680.
[29] S. Jana, A. Mondal, A. Ghosh, Appl. Catal., B 232 (2018) 26.
[30] D. Chu, F. Li, X. Song, H. Ma, L. Tan, H. Pang, X. Wang, D. Guo, B. Xiao, J. Colloid Interface Sci. 568 (2020) 130.
[31] L. Liu, J. Wang, C. Wang, G. Wang, Appl. Surf. Sci. 390 (2016) 303.
[32] F. Güneş, A. Aykaç, M. Erol, Ç. Erdem, H. Hano, B. Uzunbayir, M. Şen, A. Erdem, J. Alloys Compd. 895 (2022) 162688.
[33] A. Ghosh, D. Ganguly, R. Sundara, J. Electroanal. Chem. 895 (2021) 115386.
[34] R. Ahmad, M.-S. Ahn, Y.-B. Hahn, Electrochem. Commun. 77 (2017) 107.
[35] J. Saravanan, M. Pannipara, A.G. Al-Sehemi, S. Talebi, V. Periasamy, S.S. Shah, M.A. Aziz, G. Gnana Kumar, J. Mater. Sci.: Mater. Electron. 32 (2021) 24775.
[36] S. Phetsang, P. Kidkhunthod, N. Chanlek, J. Jakmunee, P. Mungkornasawakul, K. Ounnunkad, Sci. Rep. 11 (2021) 9302.
[37] J. Lv, C. Kong, Y. Xu, Z. Yang, X. Zhang, S. Yang, G. Meng, J. Bi, J. Li, S. Yang, Sens. Actuators B Chem. 248 (2017) 630.
[38] T. Dayakar, K.V. Rao, K. Bikshalu, V. Malapati, K.K. Sadasivuni, Biosens. Bioelectron. 111 (2018) 166.
[39] V. Archana, Y. Xia, R. Fang, G. Gnana Kumar, ACS Sustain. Chem. Eng. 7 (2019) 6707.
[40] M. Palmer, M. Masikini, L.-W. Jiang, J.-J. Wang, F. Cummings, J. Chamier, O. Inyang, M. Chowdhury, J. Alloys Compd. 853 (2021) 156900.
[41] M. Geetha, M.R. Maurya, S. Al-maadeed, A.A. Muthalif, K.K. Sadasivuni, J. Electron. Mater. 51 (2022) 4905.
[42] F. Cui, H. Sun, X. Yang, H. Zhou, Y. Wu, J. Li, H. Li, J. Liu, C. Zeng, B. Qu, J. Chem. Eng. 457 (2023) 141303.
[43] M. Figiela, M. Wysokowski, E. Stanisz, D. Hao, B.J. Ni, Electroanal. 34 (2022) 1725.
[44] Z. Shaghaghi, M. Aligholivand, R. Mohammad-Rezaei,

Int. J. Hydrogen Energy. 46 (2021) 389.
[45] Z. Shaghaghi, R. Bikas, Y. Heshmati-Sharabiani, D. Trzybiński, K. Woźniak, Photosynth. Res. 154 (2022) 369.
[46] Z. Shaghaghi, A.R. Amani-Ghadim, M. Seraji, Mater. Chem. Phys. 243 (2020) 122635.
[47] M.R. Fahlepy, Y. Wahyuni, M. Andhika, A.T. Vistarani, S. Subaer, Mater. Sci. Forum. 967 (2019) 259.
[48] J. Yoonus, R. Resmi, B. Beena, Mater. Today: Proc. 46 (2021) 2969.
[49] T. Abdullah, S.I. Shamsah, I.A. Shaaban, M. Akhtar, S. Yousaf, Synth. Met. 299 (2023) 117472.
[50] M. Farahmandjou, F. Soflaee, Phys. Chem. Res. 31 (2015) 191.
[51] D.E. Fouad, C. Zhang, H. El-Didamony, L. Yingnan, T.D. Mekuria, A.H. Shah, Results Phys. 12 (2019) 1253.
[52] S. Vignesh, S. Suganthi, M. Srinivasan, A. Tamilmani, J.K. Sundar, S. Gedi, B. Palanivel, S.F. Shaikh, M. Ubaidullah, M.K. Raza, J. Alloys Compd. 902 (2022) 163705.
[53] N.X.D. Linh, N.T. Hanh, L.M. Cuong, N.T. Huong, N.T.T. Ha, T.D. Trinh, N. Van Noi, N.T.D. Cam, T.-D. Pham, Top. Catal. 66 (2023) 139.
[54] K. Subhash, M. Benoy, J. Duraimurugan, R. Siranjeevi, S. Prabhu, Mater. Lett. 330 (2023) 133288.
[55] G.P. Singh, K. Singh, J. Singh, R.K. Jain, B. Singh, R.C. Singh, Eur. Phys. J. Plus 137 (2022) 959.
[56] C.A. Paul, E.R. Kumar, J. Suryakanth, A. Abd El-Rehim, Ceram. Int. 49 (2023) 31193.
[57] A. Abdel-Galil, N. Moussa, I. Yahia, J. Mater. Sci.: Mater. Electron. 33 (2022) 4984.
[58] S.J. Kashyap, R. Sankannavar, G. Madhu, Mater. Chem. Phys. 286 (2022) 126118.
[59] P. Muhambihai, V. Rama, P. Subramaniam, Environ. Nanotechnol. Monit. Manag. 14 (2020) 100360.
[60] P. Sathishkumar, R. Sweena, J.J. Wu, S. Anandan, J. Chem. Eng. 171 (2011) 136.
[61] S. Jafari, Z. Shaghaghi, Dalton Trans. 52 (2023) 7564.
[62] P. Nuengmatcha, P. Porrawatkul, S. Chanthai, P. Sricharoen, N. Limchoowong, J. Environ. Chem. Eng. 7 (2019) 103438.
[63] A. Kanwal, S. Sajjad, S.A.K. Leghari, Z. Yousaf, J. Phys. Chem. Solids 151 (2021) 109899.
[64] Y. Gao, N. Zhang, C. Wang, F. Zhao, Y. Yu, ACS Appl. Energy Mater. 3 (2019) 666.
[65] E.C. Pastrana, V. Zamora, D. Wang, H. Alarcón, Adv. Nat. Sci.: Nanosci. Nanotechnol. 10 (2019) 035012.
[66] D.S. Abraham, M. Chandran, M. Vinoba, R. Yamuna, M. Bhagiyalakshmi, Langmuir, 39 (2023) 4756.
[67] Z. Albu, F. Alzaid, S. AlQahtani, N. Al Abass, F. Alenazey, I. Allehyani, B. AlOtaibi, J. Colloid Interface Sci. 587 (2021) 39.
[68] F. Momeni, S.M. Khoshfetrat, K. Zarei, ACS Appl. Nano Mater. 6 (2023) 19239.
[69] S. Wang, H. Yang, X. Yi, H.M.K. Sari, X. Zhang, T. Wang, Z. Zhou, B. Cao, J. Qin, J. Wang, Appl. Surf. Sci. 574 (2022) 151649.
[70] K. Tai, X. He, X. Yuan, K. Meng, Y. Gao, F. Yuan, Colloids Surf. A: Physicochem. Eng. Asp. 518 (2017) 218.
[71] Z. Shaghaghi, S. Jafari, R. Mohammad-Rezaei, J. Electroanal. Chem. 915 (2022) 116369.
[72] J.T. Barragan, S. Kogikoski Jr, E.T. da Silva, L.T. Kubota, Anal. Chem. 90 (2018) 3357.
[73] Y. Liu, W. Zhao, X. Li, J. Liu, Y. Han, J. Wu, X. Zhang, Y. Xu, Appl. Surf. Sci. 512 (2020) 145710.
[74] C. Xia, W. Ning, Electrochem. Commun. 12 (2010) 1581.
[75] X. Cao, N. Wang, Analyst 136 (2011) 4241.
[76] X. Zhou, X. Gu, Z. Chen, Y. Wu, W. Xu, J. Bao, Sens. Actuators B: Chem. 329 (2021) 129117.
[77] H. Wu, Y. Yan, Q. Huang, G. Liang, F. Qiu, Z. Ye, D. Liu, New J. Chem. 44 (2020) 12723.
[78] S.M. Khoshfetrat, I. Chegeni, Sens. Actuators B: Chem. 397 (2023) 134668.
[79] X. Tan, J. Zhang, S. Tan, D. Zhao, Z. Huang, Y. Mi, Z. Huang, Electroanal. 21 (2009) 1514.
[80] R.A. Kamin, G.S. Willson, Anal. Chem. 52 (1980) 1198.
[81] A. Umar, R. Ahmad, A. Al-Hajry, S.H. Kim, M.E. Abaker, Y.B. Hahn, New J. Chem. 38 (2014) 5873.
[82] A. Umar, K. Singh, S.K. Mehta, H. Fouad, O.Y. Alothman, Nanosci. Nanotech. Lett. 10 (2018) 429.
[83] M. Marie, A. Manoharan, A. Kuchuk, S. Ang, M. Manasreh, Nanotech. 29 (2018) 115501.
[84] Y. Chen, H. Zhang, H. Xue, X. Hu, G. Wang, C. Wang, Mater. Sci. Eng. C 35 (2014) 420.
[85] Z. Shahnavaz, F. Lorestani, Y. Alias, P.M. Woi, Appl.

Surf. Sci. 317 (2014) 622.
[86] L. Peng, Y. Luo, H. Xiong, S. Yao, M. Zhu, H. Song, Electroanal. 33 (2021) 723.
[87] S. Yadav, N. Rani, K. Saini, Diam. Relat. Mater. 142 (2024) 110707.
[88] Y. Wang, X.Y. Liu, X. Xu, Y. Yang, L.H. Huang, Z.Y. He, Z.S. Feng, Mater. Res. Bull. 101 (2018) 340.
[89] N.M. Nor, K.A. Razak, Z. Lockman, J. Mater. Res. 35 (2020) 1279.
[90] S.M. Khoshfetrat, K. Fasihi, F. Moradnia, H.K. Zaidan, E. Sanchooli, Anal. Chim. Acta 1252 (2023) 341073.
[91] J. Noiphung, T. Songjaroen, W. Dungchai, C.S. Henry, O. Chailapakul, W. Laiwattanapaisal, Anal. Chim. Acta 788 (2013) 39.
[92] Q. Xu, Y. Zhao, J.Z. Xu, J.-J. Zhu, Anal. Chim. Acta 114 (2006) 379.